VIII International Conference on Computational Methods in Marine Engineering
MARINE 2019
R. Bensow and J. Ringsberg (Eds)

NUMERICAL MODELLING OF THE INTERACTION BETWEEN A FISH NET AND FLUID USING CFD

TOBIAS MARTIN*, ARUN KAMATH AND HANS BIHS

* Department of Civil and Environmental Engineering
Norwegian University of Science and Technology
Høgskoleringen 7a, 7491 Trondheim, Norway
e-mail: tobias.martin@ntnu.no

Key words: Fluid-structure interaction, Net modelling, Porous media, CFD

Abstract. A numerical model for the determination of the deformed shape of nets under consideration of hydrodynamic loads and elastic twines is presented. The hydrodynamic forces are incorporated using Morison's formula and force coefficients evaluated from experiments. The model is coupled to a CFD fluid model by representing the net's influence on the fluid as a porous medium. For this purpose, the volume-averaged Navier-Stokes equations, which include porosity and an additional resistance term, are solved. The source term is calculated from an adapted version of Forchheimer's equation for flow in porous media. A validation part focusing on forces and deformation of a net wall in steady current provides insight into the accuracy of the chosen concept.

1 INTRODUCTION

The aquaculture industry has seen strong growth over the last decades due to its potential to meet the rising global food demand. Offshore fish production becomes relevant as the size of the structures increases and greater concerns about the environmental impact on the nearshore zone arise. In the open sea, severe environmental loadings from high energy sea states necessitate accurate analysis of motion and fatigue for the design of reliable and economical marine fish farm structures. Separated studies on either the motion of the structure or the fluid around the structure using experimental or simple numerical tools were predominant in the past. However, these approaches are not suitable for real sea state conditions due to the strong and non-linear fluid-structure interaction. In contrast, computational fluid dynamics can be applied to understand the structural and environmental challenges in the operation of the whole structures by studying the forces on and the fluid dynamics in and around the cages.

Several experimental studies were presented for nets in current. Patursson [1] published a series of measurements of drag and lift forces on a fixed net panel and the velocity reduction behind the net for different inflow velocities and angles between fluid and panel. Similar studies were presented in [2] where the authors investigated the deformation of a square net in different current velocities. Lader and Enerhaug [3] analysed the forces and deformation of a net cage in

current. They found a strong coupling between occurring forces and deformation and concluded that existing simple drag formulae for stiff net panels are not suitable for calculating the forces on flexible cage structures. Less research focused on experiments including waves. Lader et al. [4, 5] studied wave forces on net panels in a small wave flume and compared the results with different wave force models. They could show the increasing influence of the net on the wave with increasing wave steepness. A complete study of a net cage in current and waves including an elastic floater, mooring and net is presented in [6], where the authors investigated the validity of different rational hydrodynamic load models for more complex wave situations.

The numerical representation of the net is mostly based on a finite element method (FEM). Tronstad [7] developed a non-linear FEM applying membrane elements suitable for static analyses of net deformation. Priour [8] generalised this idea for triangular elements and in [9], a similar approach is used for dynamic calculations. All the approaches rely on super elements which represent a certain area of the net. In contrast, Tsukrov et al. [10] presented a consistent net element method. Here, the discrete net consists of several 1D truss elements which move due to tension and external forces from a modified Morison equation. Marichal [11] developed an elastic truss element method with kinematic constraints. A similar approach is presented in [12]. It is a quasi-static approach which leads to an efficient overall computation due to missing time step restrictions. The coupling of a net model to a fluid solver is advanced by different researches. Patursson et al. [13] incorporated the net as a porous medium and solved the volume-averaged Navier-Stokes equations. Good agreements with experiments for a fixed net panel could be shown, but the deformation of the net is not included in the study. Bi et al. [2] and Zhao et al. [14] followed the same approach but included the net deformation using a lumped-mass model. They validated the model for current and waves and could show good agreement with the experiments. Chen and Christensen [15, 16] extended this idea for net cages and provided a comprehensive validation of their approach. The good accuracy of the model for current cases shows the validity of this approach.

The presented net model is implemented in the open-source CFD code REEF3D [17]. The fluid solver has been validated for a wide range of marine applications which are relevant for this research. Kamath et al. [18] tested successfully the code for shoaling and decomposition of non-breaking and breaking waves over varying bathymetry. In [19], the code showed good agreement with experiments for the fluid-structure interaction with fixed cylinders. Further, floating structures [20] including a numerical mooring model [21] were incorporated using a directional immersed boundary method. In the following, details about the numerical fluid and net models are given. The coupling between the two models is mainly based on the ideas in [13, 16]. The paper concludes with a validation of the presented approach for the deformation of a net in current and the forces acting on the net.

2 NUMERICAL MODELS

2.1 Fluid model

The Reynolds averaged continuity equation and Navier-Stokes (RANS) equations for incompressible fluids are the typical set of equations solved for describing the fluid. In non-conservative

term, they are given as

$$\frac{\partial u_i}{\partial x_i} = 0,$$
$$\frac{\partial u_i}{\partial t} + u_j \frac{\partial u_i}{\partial x_j} = -\frac{1}{\rho}\frac{\partial p}{\partial x_i} + \frac{\partial}{\partial x_j}\left(\nu_{\text{eff}}\left(\frac{\partial u_i}{\partial x_j} + \frac{\partial u_j}{\partial x_i}\right)\right) + g_i, \tag{1}$$

with u_i the velocities in the principal directions, p including the pressure and the root mean square of the turbulent velocity fluctuations, and $\vec{g}$ accounting for gravitational forces. In a two phase approach, the density ρ and the viscosity ν_{eff} have to be determined from the two material properties. The effective viscosity is the sum of the kinematic viscosity ν and the turbulent viscosity ν_t, which is calculated using Boussinesq's approximation and the two-equations $k-\varepsilon$ turbulence model.

The set of equations (1) is computed on a rectilinear staggered grid using a finite difference method. Chorin's projection method for incompressible flows [22] is implemented with a third-order accurate Runge-Kutta discretisation scheme for temporal terms [23] and a fifth-order accurate weighted essentially non-oscillatory (WENO) scheme [24] for convection terms. The resulting Poisson equation for pressure is solved by HYPRE's MPI parallelized BiCGStab method [25] with a geometric multigrid method as preconditioner.

Resolving the twines of the net would incorporate a very large number of cells. Therefore, the effect of the net on the fluid is incorporated as a porous medium. For this purpose, a volume averaging operator according to

$$\langle a \rangle = \frac{1}{V}\int_{V_f} a \; dV, \tag{2}$$

is introduced. The portion fluid volume V_f in the control volume V is expressed trough the porosity Φ which is defined as

$$\Phi = \frac{V_f}{V}, \quad (\Phi \in [0,1]). \tag{3}$$

Without presenting the derivation, the introduction of the operator in (1) results in the volume-averaged RANS (VARANS) equations [26]

$$\frac{\partial \langle u_i \rangle}{\partial x_i} = 0,$$
$$(1+c_a)\frac{\partial}{\partial t}\frac{\langle u_i \rangle}{\Phi} + \frac{\langle u_j \rangle}{\Phi}\frac{\partial}{\partial x_j}\frac{\langle u_i \rangle}{\Phi} = -\frac{1}{\rho}\frac{\partial \langle p \rangle}{\partial x_i} + \frac{1}{\Phi}\frac{\partial}{\partial x_j}\left(\nu_{\text{eff}}\left(\frac{\partial \langle u_i \rangle}{\partial x_j} + \frac{\partial \langle u_j \rangle}{\partial x_i}\right)\right) + g_i + S_i. \tag{4}$$

The added mass coefficient c_a takes the transient interaction of fluid and twines into account but is not well investigated for nets yet. In this study, the value is calculated as given in [15]. The source term S_i includes the drag resistance of the porous zone and can be calculated under consideration of the equation of Forchheimer as [13]

$$S_i = -\rho \cdot \left(\nu D_{ij} \langle u_i \rangle + \frac{1}{2} C_{ij} | \langle u \rangle | \langle u_j \rangle\right). \tag{5}$$

The material matrices D_{ij} and C_{ij} include the porous media resistance coefficients in normal and tangential directions of a net element in there main diagonal. If the element is not aligned with the principal directions of the fluid flow, a coordinate transformation as given in [13] is applied to the matrices.

2.2 Net model

In this paper, the tension element method [12] is utilised for the simulation of the deformation of a net plane. It is assumed that the net consists of square meshes such that the solidity ratio S can be approximated as [27]

$$S = \frac{2d}{l} - \left(\frac{d}{l}\right)^2, \tag{6}$$

where d is the diameter and l is the length of each twine. The porosity defined in (3) equals then $1 - S$.

The net is represented as a finite number of massless bars connected with mass points P. Further, the elasticity of the twines is incorporated, and bending stiffness is neglected such that a flexible system is assumed. A static force equilibrium can then be stated for each of the N_{ik} inner knots of the net $P^{(\nu)}$ as (see Fig. 1)

$$\sum_{j=1}^{N_{b,\nu}} \left(\vec{f}^{(j)} T^{(j)} + \frac{1}{2} \cdot \vec{H}^{(j)}\right) + \vec{G}^{(\nu)} = \vec{0}, \quad \nu = 1, ..., N_{ik}. \tag{7}$$

Here, the $N_{b,\nu}$ bars which are connected to $P^{(\nu)}$ point in the direction of the unit vectors $\vec{f}$ and include the tension forces T. Once these forces are known for each of the bars, the length can be updated from e.g. Hooke's law

$$l^{(j)} = l_0^{(j)} \cdot \left(1.0 + \frac{T^{(j)}}{EA}\right). \tag{8}$$

The gravity forces $\vec{G}$ are known forces and uniformly distributed on all knots. The hydrodynamic forces $\vec{H}$ are calculated from the surrounding fluid using Morsion's drag formula

$$\vec{H}^{(j)} = \frac{\rho d l^{(j)}}{2} \cdot \left[c_n \left(\vec{v} - \left(\vec{v} \cdot \vec{f}\right) \vec{f}\right) \left|\vec{v} - \left(\vec{v} \cdot \vec{f}\right) \vec{f}\right| + c_t \left(\vec{v} \cdot \vec{f}\right) \left|\vec{v} \cdot \vec{f}\right| \cdot \vec{f}\right]^{(j)}, \tag{9}$$

with c_n and c_t the normal and tangential drag coefficients. The chosen velocity $\vec{v}$ is due to the fluid because of the quasi-static assumption for the net motion. The coefficients are calculated using formulae for flow around cables [28]

$$c_n = \begin{cases} \frac{8\pi}{\mathrm{Re} \cdot s} \cdot \left(1 - 0.87 s^{-2}\right), & (0 < \mathrm{Re} \leq 1) \\ 1.45 + 8.55 \cdot \mathrm{Re}^{-0.9}, & (1 < \mathrm{Re} \leq 30) \\ 1.1 + 4 \cdot \mathrm{Re}^{-0.5}, & (30 < \mathrm{Re} \leq 10^5) \end{cases},$$

$$c_t = \pi 1.05^{-3} \cdot \left(0.55\sqrt{\mathrm{Re}} + 0.084 \cdot \mathrm{Re}^{\frac{2}{3}}\right), \tag{10}$$

with $s = -0.077215665 + \ln(\frac{8}{\mathrm{Re}})$ and $\mathrm{Re} = \frac{v_n d}{\nu}$. The same approach was used by Tsukrov et al. [10] for developing their consistent net element model.

The solution of (7) is found by separating internal and external forces. This leads to

$$\sum_{j=1}^{N_{b,\nu}} \left(\vec{f}^{(j)} T^{(j)}\right) = \sum_{j=1}^{N_{b,\nu}} \frac{1}{2} \cdot \vec{H}^{(j)} + \vec{G}^{(\nu)}, \quad \nu = 1, ..., N_{ik}. \tag{11}$$

The arising system of equations is solved for the unit bar vectors using a successive approximation method. A net of rectangular meshes always contains more twines than knots such that the system is undetermined. To overcome this issue and include physical coherence into the model, appropriate geometrical constraints in form of boundary and internal mesh equations are added as described in [12].

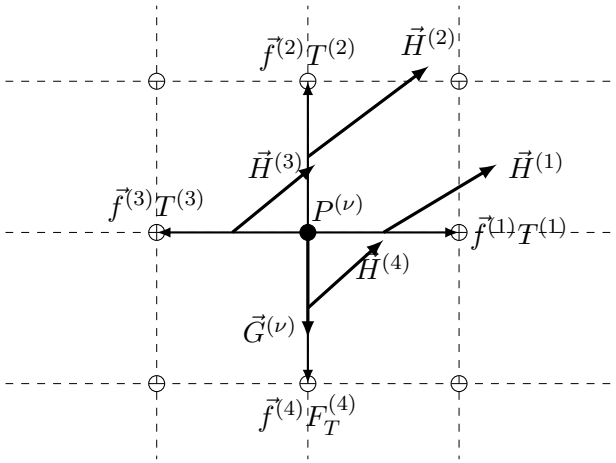

Figure 1: Acting forces at knot P^{ν} of the net.

2.3 Coupling algorithm

The algorithm developed for simulating the fluid-structure interaction of a moving net is shown in figure 2. In the first step of the iterative process of the net model, the hydrodynamic forces are updated using (9) and (10). The necessary fluid velocity information is provided by interpolating the velocity field at all knots of the net and averaging them accordingly for each intermediate bar. Additionally, the elasticity of the twines is incorporated using (8). The system is then solved and corrected as described above, and the new net position is stored when convergence has been reached. In the fluid solver, a zone of porous medium is then generated based on the current position of the net. Here, the authors follow the idea of Chen and Christensen [16], which defines prisms of thickness t around the triangulated net and checks for each fluid cell whether it is within these prisms. Due to the time and space dependency of the angles of attack, the porous media resistance coefficients have to be calculated for each mesh in each time step. The drag resistance is then determined for each cell in the porous zone using the coefficients from the corresponding mesh and (5). A porosity value is assigned, and the fluid problem is solved with the VARANS equations as given in section 2.1.

3 VALIDATION

For validation purposes, two cases are compared to experimental data from the literature. For both cases, the resistance coefficients are taken from [13]. They are based on comparisons between a simple analytical model and experimental data for nets with different solidity.

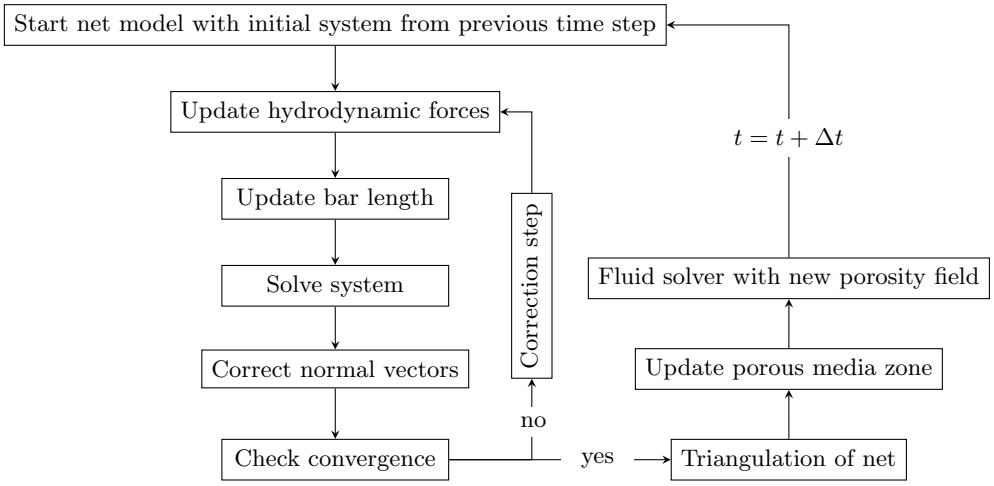

Figure 2: Flowchart of the presented fluid-structure interaction algorithm.

3.1 Fixed net panel in steady current flow

A fixed net panel in current flow under several angles of attack α and current velocities shall be compared to the experimental data of Patursson et al. [13]. Here, the drag and lift force coefficients and the velocity reduction factor behind the net u_r are considered. The latter is defined as

$$u_r = \frac{u_\infty - u_{2.5}}{u_\infty}, \tag{12}$$

with $u_{2.5}$ the measured velocity $2.5m$ behind the net. The force coefficients are calculated by integrating the source term in x- and z-direction over the porous zone

$$c_d = \frac{S_x t A}{\frac{\rho}{2} A u_\infty^2}, \quad c_l = \frac{S_z t A}{\frac{\rho}{2} A u_\infty^2}. \tag{13}$$

The thickness of the zone is set to be $50mm$. The net is fixed in a frame of $1m \times 1m$ and has a solidity of 0.184. Three different angle of attacks, i.e. $\alpha = 15°, 45°, 90°$ and four different inflow velocities between $0.125m/s$ and $0.75m/s$ are investigated. The chosen porous resistance coefficients are $C_{11} = 5.098, C_{22} = C_{33} = 1.6984$ and $D_{11} = 51730, D_{22} = C_{33} = 26379$. A computational domain of $4.5m \times 3.66m \times 2.44m$ consisting of 0.6Mio. cells is chosen. The nets middle position is kept at $(1.5m, 1.83m, 1.22m)$ for all angle of attacks.

A slice of the domain at $y = 0.915m$ is shown for the different angles of the net and $u_\infty = 0.5m/s$ in Fig. 3. The wake of the net is clearly visible and has approximately the same width as the net panel. At $\alpha = 15°$ some fluid is accelerated alongside the net and flows below the panel. As the angle of attack increases, the fluid slows down in front of the net which leads to a decreasing velocity at the net itself. Behind the net, a nearly steady velocity can be observed for all angles of attack. Fig. 4a shows the velocity reduction factor for the different angles of attack and velocities. A very good agreement can be achieved at $\alpha = 45°$ for the whole range of velocities. For $\alpha = 90°$, the numerical model over-predicts the experimental results

with about 50%. In contrast, the model under-predicts the experiment at a small α. The observed offset hints at a good agreement of the chosen distribution of drag forces with respect to Reynolds numbers but a less accurate incorporation of the angle between the fluid and net element. Further research has to clarify this issue. A similar situation can be seen for the force coefficients, shown in Fig. 4b and Fig. 4c. Again, a small over-prediction can be seen for $\alpha = 15°$ and a small under-prediction for $\alpha = 90°$. However, the calculated distributions match well the experimental data with errors less than 20%.

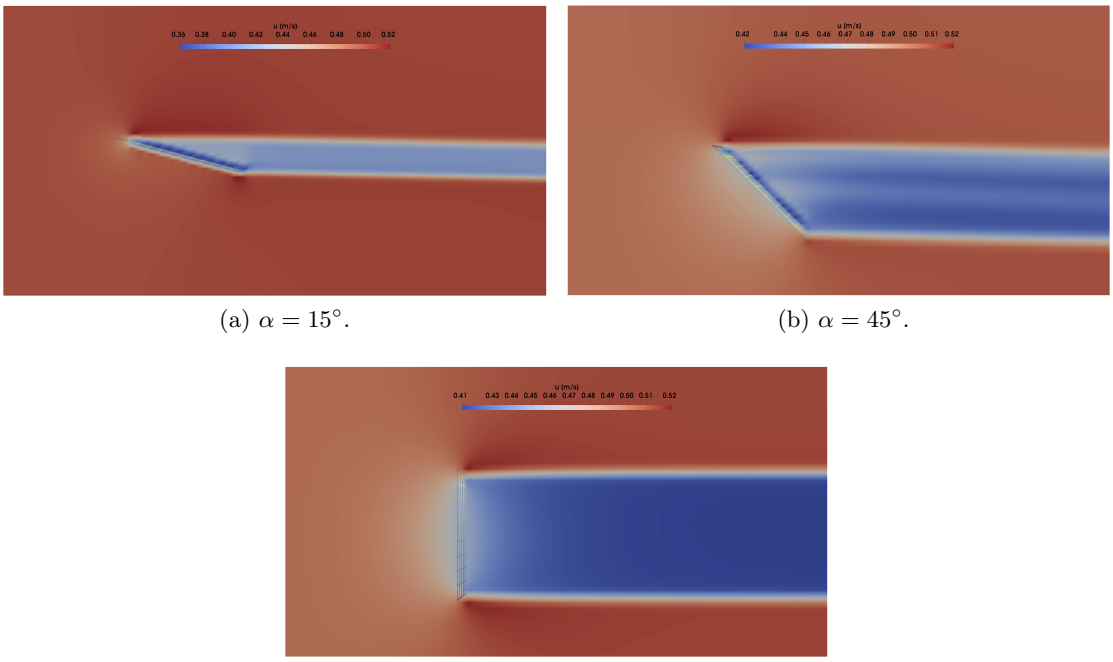

(a) $\alpha = 15°$.

(b) $\alpha = 45°$.

(c) $\alpha = 90°$.

Figure 3: Velocity field for the fixed net panel in steady current flow of $u_\infty = 0.5m/s$.

3.2 Moving net panel in current

The motion of a net panel in steady current shall be analysed next. For this purpose, the experimental setup from [2] for the inflow velocity of $0.226m/s$ is taken as the reference. The net is fixed on the top, and sinker with a weight of $64.5g$ in water is attached to the bottom. It has a size of $0.3m \times 0.3m$ and consists of 225 square meshes. Each twine has a diameter of $2.6mm$ and a length of $20mm$. This results in a solidity of 0.26. Further, the chosen material has a density of $1150kg/m^3$ which leads to small gravity forces in water. In the numerical simulations, the geometry of the net is not changed which prevents eventual scaling effects. The sinker is represented by distributing its weight equally to the bottom knots. The porous resistance coefficients are taken from above, whereas the thickness of the zone is reduced to $20mm$. The three-dimensional computational domain is illustrated in Fig. 5a. The domain has a length of $1.5m$, a width of $0.5m$ and a height of $0.6m$. The numerical grid consists of $0.72Mio$ cells with

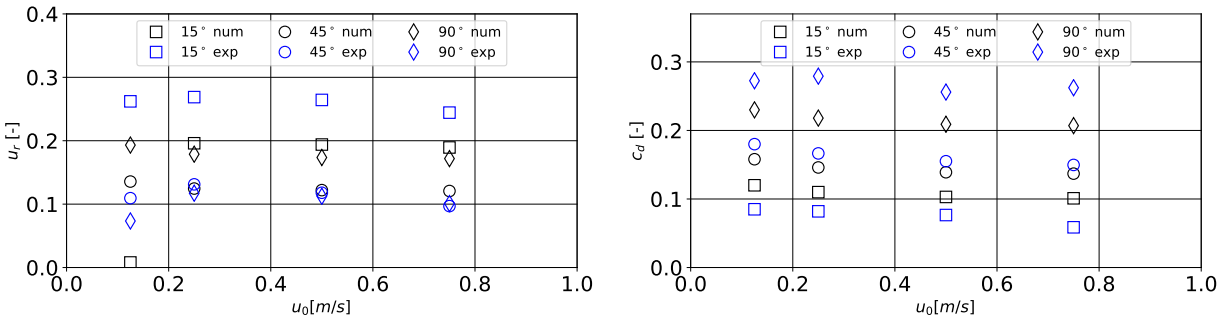

(a) Velocity reduction factor u_r.

(b) Drag coefficient c_d.

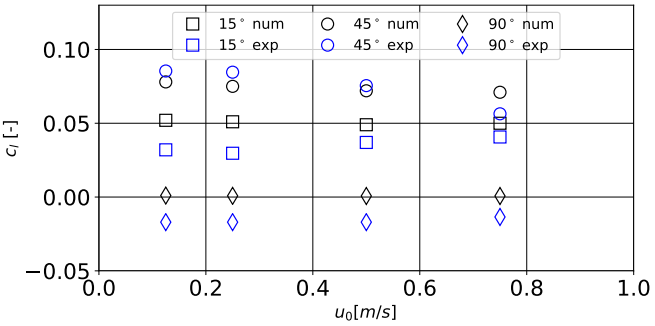

(c) Lift coefficient c_l.

Figure 4: Comparison of numerical and experimental results for the fixed net panel in steady current flow.

gradual refinement around the net. The top bar of the net is fixed in the middle of the tank at $x = 0.5m$ and $z = 0.4m$. In accordance with the experiments, no free surface is taken into account.

The loss of momentum due to the drag of the net is analysed in Fig. 5b. Here, the predicted velocity distribution along the x-axis through the points $(y, z) = (0.25, 0.25)$ is shown. The wake velocity behind the net reproduces the experimental data which indicates properly chosen porous resistance coefficients. The deformation of the net panel is presented in Fig. 6. The displacement of the net bottom is in good agreement with the experiments for the x-direction. In z-direction, the numerical model is $50mm$ over the experimental results. This is caused by a generally over-prediction of drag and lift forces, which result in a more significant bending of the net geometry.

As a final remark, the tension forces in the net can be seen in Fig. 5a. The highest tension is computed in the upper part of the net where the weight of the net and the sinker is acting in combination with relatively large shear forces due to the small angle between net and fluid. The smallest tension is predicted in the lowest part of the net due to a smaller weight acting on these meshes. In addition, the ideal flexible assumption prevents the eventual occurrence of bending or shear forces in this part.

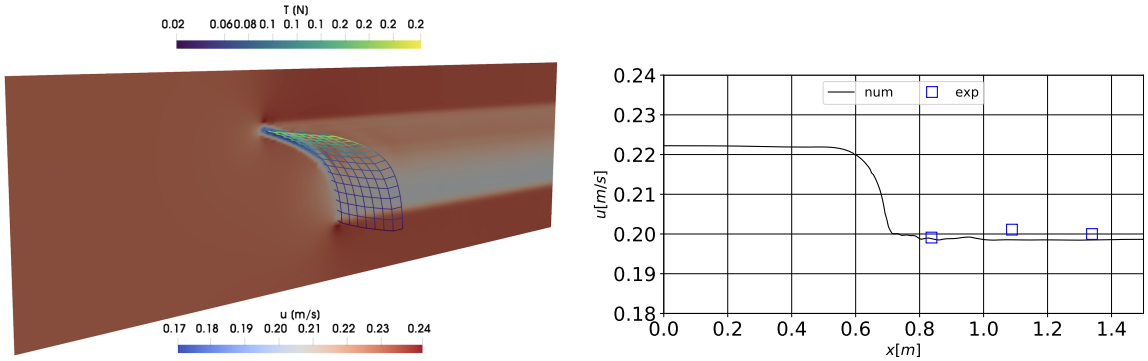

(a) Velocity distribution and tension forces in deformed net panel.

(b) Velocity u over x at $(y, z) = (0.25, 0.25)$. Compared to the experimental results [2]

Figure 5: Results of the simulation of a net panel deformation in steady current.

4 CONCLUSIONS

This paper presents a numerical approach for the simulation of the fluid-structure interaction of a net and fluid. The applied tension element method is based on static force equilibria at each knot of the net and additional geometrical constraints to close the system of equations. Hence, a fast and reliable solution procedure for quasi-stationary problems is provided. The coupling between fluid and structural model is achieved by a porous medium introduction into the fluid describing equations. This approach has the advantage of being easy to implement and highly adaptable to various net configurations. The validation of the algorithm indicated the successful implementation but also several discrepancies in comparison to experimental data. Here, the driving factors are the calculation of forces on the net from the surrounding fluid and the porous resistance coefficients which have to be determined from a limited amount of experiments. These indications were also concluded in previous studies, and are especially distinct for more complex structures, such as net cages, and in wave conditions. Therefore, an improvement of these leading factors has to be sought during further research.

5 ACKNOWLEDGMENT

The authors are grateful for the grants provided by the Research Council of Norway under the Havbruk2 project (No. 267981). This research was supported in part with computational resources at NTNU provided by The Norwegian Metacenter for Computational Sciences (NOTUR, http://www.notur.no) under project no. NN2620K.

REFERENCES

[1] Patursson, Ø., 2007. Tow tank measurements of drag- and lift force on a net panel and current reduction behind the net panel. Technical Report NVDRit2007:10, University of the Faroe Islands, Torshavn, Faroe Islands.

[2] Bi, C.-W., Zhao, Y.-P., Dong, G.-H., Xu, T.-J., and Gui, F.-K., 2014. "Numerical simulation of the interaction between flow and flexible nets". *J. Fluids Struct.*, ***45***, pp. 180–201.

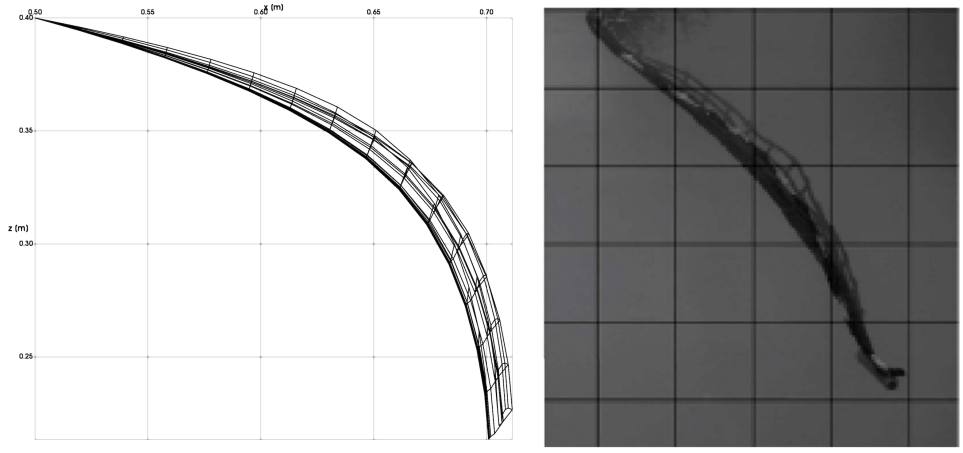

(a) Numerical predicted net deformation.

(b) Experimental result taken from [16] for comparison. Each mesh has a length of $50mm$.

Figure 6: Comparison of numerical and experimental deformation of a net in steady current.

[3] Lader, P. F., and Enerhaug, B., 2005. "Experimental investigation of forces and geometry of a net cage in uniform flow". *IEEE Journal of Oceanic Engineering,* ***30***(1), pp. 79–84.

[4] Lader, P., Jensen, A., Sveen, J. K., Fredheim, A., Enerhaug, B., and Fredriksson, D., 2007. "Experimental investigation of wave forces on net structures". *Applied Ocean Research,* ***29***(3), pp. 112–127.

[5] Lader, P. F., Olsen, A., Jensen, A., Sveen, J. K., Fredheim, A., and Enerhaug, B., 2007. "Experimental investigation of the interaction between waves and net structures—Damping mechanism". *Aquacultural Engineering,* ***37***(2), pp. 100–114.

[6] Kristiansen, T., and Faltinsen, O. M., 2015. "Experimental and numerical study of an aquaculture net cage with floater in waves and current". *Journal of Fluids and Structures,* ***54***, pp. 1–26.

[7] Tronstad, H., 2000. Nonlinear Hydroelastic Analysis and Design of Cable Net Structures Like Fishing Gear Based on the Finite Element Method. Ph.D. thesis, Norwegian University of Science and Technology, Faculty of Marine Technology.

[8] Priour, D., 1999. "Calculation of net shapes by the finite element method with triangular elements". *Commun. Numer. Meth. Engng.,* ***15***, pp. 757–765.

[9] Lader, P. F., and Fredheim, A., 2006. "Dynamic properties of a flexible net sheet in waves and current—A numerical approach". *Aquacultural Engineering,* ***35***(3), pp. 228–238.

[10] Tsukrov, I., Eroshkin, O., Fredriksson, D., Swift, M. R., and Celikkol, B., 2003. "Finite element modeling of net panels using a consistent net element". *Ocean Engineering,* ***30***, pp. 251–270.

[11] Marichal, D., 2003. Cod-end numerical study. In: 3rd International Conference on Hydroelasticity in Marine Technology, Oxford, UK.

[12] Martin, T., Schacht, S., Riesen, P., and Paschen, M., 2018. "Efficient implementation of a numerical model for flexible net structures". *Ocean Engineering,* ***150***, pp. 272–279.

[13] Patursson, Ø., Swift, M. R., Tsukrov, I., Simonsen, K., Baldwin, K., Fredriksson, D., and Celikkol, B., 2010. "Development of a porous media model with application to flow through and around a net panel". *Ocean Engineering,* ***37***, pp. 314–324.

[14] Zhao, Y.-P., Bi, C.-W., Liu, Y.-X., Dong, G.-H., and Gui, F.-K., 2014. "Numerical Simulation of Interaction Between Waves and Net Panel Using Porous Media Model". *Engineering Applications of Computational Fluid Mechanics,* ***8***(1), pp. 116–126.

[15] Chen, H., and Christensen, E., 2016. "Investigations on the porous resistance coefficients for fishing net structures". *J. Fluids Struct.,* ***65***, pp. 76–107.

[16] Chen, H., and Christensen, E., 2017. "Development of a numerical model for fluid-structure interaction analysis of flow through and around an aquaculture net cage". *Ocean Engineering,* ***142***, pp. 597–615.

[17] Bihs, H., Kamath, A., Chella, M. A., Aggarwal, A., and Arntsen, Ø. A., 2016. "A new level set numerical wave tank with improved density interpolation for complex wave hydrodynamics". *Computers & Fluids,* ***140***, pp. 191–208.

[18] Kamath, A., Chella, M. A., Bihs, H., and Arntsen, Ø. A., 2017. "Energy transfer due to shoaling and decomposition of breaking and non-breaking waves over a submerged bar". *Engineering Applications of Computational Fluid Mechanics,* ***11(1)***, pp. 450–466.

[19] Kamath, A., Chella, M. A., Bihs, H., and Arntsen, Ø. A., 2015. "Evaluating wave forces on groups of three and nine cylinders using a 3D numerical wave tank". *Engineering Applications of Computational Fluid Mechanics,* ***9***, pp. 343–354.

[20] Bihs, H., and Kamath, A., 2017. "A combined level set/ghost cell immersed boundary representation for floating body simulations". *Int. J. Numer. Meth. Fluids,* ***83***, pp. 905–916.

[21] Martin, T., Kamath, A., and Bihs, H., 2018. "Modelling and Simulation of Moored-floating Structures using the Tension-Element-Method". *ASME 2018 37th International Conference on Ocean, Offshore and Arctic Engineering,* ***2***.

[22] Chorin, A., 1968. "Numerical solution of the Navier-Stokes equations". *Mathematics of Computation,* ***22***, pp. 745–762.

[23] Shu, C., and Osher, S., 1988. "Efficient implementation of essentially non-oscillatory shock-capturing schemes". *Journal of Computational Physics,* ***77(2)***, pp. 439–471.

[24] Jiang, G., and Shu, C., 1996. "Efficient implementation of weighted ENO schemes". *Journal of Computational Physics,* ***126(1)***, pp. 202–228.

[25] van der Vorst, H., 1992. "BiCGStab: A fast and smoothly converging variant of Bi-CG for the solution of nonsymmetric linear systems". *SIAM Journal of Scientific Computing,* ***13***, pp. 631–644.

[26] Jensen, B., Jacobsen, N., and Christensen, E., 2014. "Investigations on the porous media equations and resistance coefficients for coastal structures". *Coastal Engineering,* ***84***, pp. 56–72.

[27] Fredheim, A., 2005. Current Forces on Net Structures. Ph.D. thesis, Norwegian University of Science and Technology, Faculty of Marine Technology.

[28] Choo, Y., and Casarella, M., 1971. "Hydrodynamics resistance of towed cables". *Journal of Hydronautics,* ***5***, pp. 126–131.